Elucidation of Anchoring and Restructuring Steps during Synthesis of Silica-Supported Vanadium Oxide Catalysts

CHEMISTRY OF MATERIALS

Article

pubs.acs.org/cm

Elucidation of Anchoring and Restructuring Steps during Synthesis of Silica-Supported Vanadium Oxide Catalysts

Alyssa M. Love,[†] Carlos A. Carrero,[†] Alessandro Chieregato,[†] Joseph T. Grant,[†] Sabrina Conrad,[†,§] René Verel,[§] and Ive Hermans*[,†,‡]

[†]Department of Chemistry, University of Wisconsin−Madison, 1101 University Avenue, Madison, Wisconsin 53706, United States

[‡]Department of Chemical and Biological Engineering, University of Wisconsin−Madison, 1415 Engineering Drive, Madison, Wisconsin 53706, United States

[§]Department of Chemistry and Applied Biosciences, ETH Zurich, Vladimir Prelog Weg 2, 8093 Zurich, Switzerland

Supporting Information

ABSTRACT: We investigate the chemical reactions involved during the synthesis of supported vanadium oxide catalysts using chemical grafting of vanadium oxytriisopropoxide ($VO(O^iPr)_3$) to thermally pretreated silica under solvent-free conditions. $VO(O^iPr)_3$ is found to react with both site-isolated silanol (Si−OH) groups and strained siloxane (≡Si−O−Si≡) bridges at the silica surface. Solid-state ^{51}V and ^{13}C MAS NMR confirms the formation of two slightly different vanadium species associated with the two anchoring mechanisms. *In situ* diffuse reflectance infrared Fourier transform spectroscopy (DRIFTS), *in situ* Raman spectroscopy, and thermogravimetric analysis-differential scanning calorimetry-mass spectrometry (TGA-DSC-MS) were used to study the subsequent calcination, revealing the formation of a transient V—OH intermediate upon the release of propene, followed by the formation of isolated VO_4 surface species upon elimination of water. X-ray absorption spectroscopy (XAS) and ^{51}V MAS NMR of the calcined material confirm the conversion of the two original vanadium sites to a species with a single isotropic shift, confirming the formation of isolated, tetrahedral VO_4 sites.

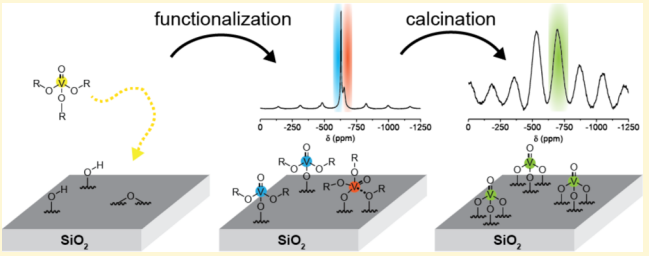

INTRODUCTION

Supported metal oxide catalysts, such as supported vanadium oxide, facilitate a variety of important chemical transformations including selective oxidations[1] and reductions.[2,3] The precise nature of the metal oxide surface structure ultimately dictates the catalytic activity of the material. For example, a supported vanadium oxide catalyst composed of only dispersed vanadium oxide species (i.e., submonolayer metal oxide sites bound directly to the support surface) will often result in different catalytic reactivity than a catalyst that also contains supported V_2O_5 nanoparticles. The oxidative dehydrogenation of propane (ODHP) reaction can be taken as a case study in this context.[1] Supported vanadium oxide catalysts containing only dispersed vanadium oxide species favor the direct dehydrogenation pathway to propene, whereas catalysts containing V_2O_5 nanoparticles accelerate the rate of overoxidation of propene to CO_x, thus lowering selectivity to propene.[4] In an effort to elucidate such structure−reactivity relationships, the nature of the supported vanadium oxide species has been rigorously investigated by a number of techniques such as UV−visible spectroscopy,[5−8] Raman spectroscopy,[7−11] Infrared (IR) spectroscopy,[6,7] X-ray absorption spectroscopy (XAS),[7,12−14] and solid-state NMR.[9,15−19] The focus of the characterization studies listed above is largely toward understanding the structure of the material, under a wide variety of conditions. However, as an alternative approach, a molecular-level understanding of the controlling chemistry during surface functionalization could serve to improve the material synthesis, e.g., to maximize the formation of desired supported metal oxide sites and/or to immobilize different metal oxides with molecular precision using scalable technology.

To a large extent, choice of synthesis procedure influences the type of vanadium oxide surface structure of the final supported catalyst.[4] Common synthesis procedures for these materials include (i) solution-based techniques such as wet impregnation and ion exchange,[4,20,21] and (ii) deposition techniques such as chemical grafting[13,14,22−26] and atomic layer deposition (ALD).[27−30] In each of these synthesis techniques, a vanadium precursor is introduced to an oxide support material. In most cases (with the exception of a few of the mentioned grafted materials[13,22−24]), the initial functionalization is followed by calcination at high temperatures (>500 °C) in order to eliminate the native metal precursor ligands and form the supported metal oxide surface species.

Received: May 26, 2016
Revised: June 10, 2016
Published: June 13, 2016

DOI: 10.1021/acs.chemmater.6b02118
Chem. Mater. 2016, 28, 5495−5504

Among the different preparation methods for supported metal oxides, grafting has shown versatility as a technique to monitor the transformation of the metal oxide precursor to dispersed metal oxide surface species.[23,24,31,32] Grafting, along with other vapor-phase deposition techniques like ALD, enable better control over the dispersion of metal oxides sites compared to wet impregnation due to the fact that anchoring of the metal precursor is limited to the number of initially available chemisorbing anchoring sites on the support.[33] In the case of silica-supported materials, the number of anchoring sites available during grafting is often controlled by the thermal pretreatment of silica.[13,23,24,26,31,32] Thermal pretreatment controls the average surface density of silanol (Si−OH) groups, generally assumed to be the predominant anchoring points on the support. Depending on the metal precursor used, strained siloxane (≡Si−O−Si≡) bridges generated during the dehydration of silica at high temperatures can also act as anchoring sites during grafting.[31,32,34]

In the present contribution, we investigate the anchoring and subsequent thermal reconstruction of vanadium oxide on amorphous silica as a representative case study for the steps governing the formation of supported metal oxide sites. We synthesized silica-supported vanadium oxide via the solvent-free vapor deposition of $VO(O^iPr)_3$ to silica dehydrated at 700 °C ($SiO_{2(700)}$). This particular vanadium precursor was chosen due to its wide use in both solution and deposition-based synthesis procedures for supported vanadium oxide. To gain insights into the elementary anchoring and restructuring steps during functionalization of the silica support, we characterized the structure of the vanadium sites on the silica support before, during, and after calcination. The surface sites on the initially grafted material ($V/SiO_{2(700)}$) were characterized using a combination of transmission FT-IR spectroscopy, X-ray absorption near edge structure (XANES) analysis, and solid-state ^{13}C and ^{51}V magic angle spinning (MAS) NMR spectroscopy. These same techniques were also applied to $VO(O^iPr)_3$ grafted on a presilylated support ($V/TMS\text{-}SiO_{2(700)}$) in order to investigate specifically the anchoring of the vanadium precursor to strained siloxane bridges. The conversion of grafted vanadium sites to their final, metal oxide surface structures was monitored using various *in situ* techniques, including diffuse reflectance infrared Fourier transform spectroscopy (DRIFTS), Raman spectroscopy, and thermogravimetric analysis-differential scanning calorimetry-mass spectrometry (TGA-DSC-MS). The vanadium structure on the grafted, calcined material and its presilylated counterpart ($V/SiO_{2(700)}\text{-}O_2$ and $V/TMS\text{-}SiO_{2(700)}\text{-}O_2$, respectively) were characterized with a combination of solid-state ^{51}V MAS NMR, and XANES analyses. In addition, $V/SiO_{2(700)}\text{-}O_2$ was also tested for the ODHP reaction as a probe reaction to both demonstrate the catalytic applicability of this grafted material and to verify the sole presence of dispersed, two-dimensional vanadium oxide species. Precisely synthesized materials, such as the supported vanadium oxide system described in this work, represent "model" catalyst systems that can be used toward understanding the structure and dispersion of surface species on a wider library of supported materials.

EXPERIMENTAL SECTION

Materials Synthesis. Silica powder (Aerosil 200 from Degussa, specific surface area of 200 $m^2 \cdot g^{-1}$) was impregnated with water and dried overnight at 100 °C in a vacuum oven. Afterward, the material was dehydrated at 200−800 °C (16 h) at 15 μbar dynamic vacuum and stored inside a glovebox (<1 ppm of O_2 and H_2O) in order to avoid readsorption of water. These materials are denoted as $SiO_{2(X)}$, with X referring to the dehydration temperature.

$VO(O^iPr)_3$ (Sigma-Aldrich, distilled two times before use, colorless) was deposited onto 300 mg of thermally pretreated silica (10 equiv based on initial silanol content) at ca. 20 μbar dynamic vacuum. The transfer phase (1 h) was followed by a reaction phase at room temperature (30 min) and a mild thermal post-treatment at 50 °C and 20 μbar dynamic vacuum (1 h) in order to evaporate the excess of $VO(O^iPr)_3$ (material denoted as $V/SiO_{2(X)}$). Samples were subsequently calcined in an air flow at 600 °C for 3 h (material denoted as $V/SiO_{2(700)}\text{-}O_2$) and dehydrated for further use (300 °C, 3 h, 20 μbar dynamic vacuum).

N,*N*-Bis(trimethylsilyl)methylamine, or $(TMS)_2NMe$, (Sigma-Aldrich, distilled two times before use) was used for the silylation of the dried silica (material denoted as $TMS\text{-}SiO_{2(X)}$). The silylating agent was exposed to the dried silica under 20 μbar vacuum in the same way as $VO(O^iPr)_3$ (using 5 equiv based on initial silanol content) and thermally post-treated at 250 °C. Afterward, $VO(O^iPr)_3$ was deposited on the silylated material to obtain $V/TMS\text{-}SiO_{2(X)}$ (5 equiv based on initial silanol content).

Materials Characterization. The vanadium content was quantified with ICP-OES (Optima 2000 DV from PerkinElmer) after digestion of the samples in HF.

Infrared spectra were recorded on a self-supporting wafer using a Bruker Alpha spectrometer in transmission mode (resolution of 2 cm^{-1}). Intensities were normalized to the Si−O−Si overtones of the silica framework. Analysis was carried out inside a glovebox (<1 ppm of H_2O and O_2).

The DRIFTS spectra were recorded by averaging 32 scans with a resolution of 8 cm^{-1}. The DiffusIR accessory (PIKE Technologies) was flushed with synthetic air at a flow rate of ca. 20 mL min^{-1} and heated at a heating rate of 20 °C·min^{-1} up to a temperature of 600 °C. The DRIFTS sample holder was filled and sealed in a glovebox (<1 ppm of O_2 and H_2O) prior to measurement.

Solid-state ^{13}C NMR and ^{51}V-NMR spectra were acquired on an Avance IIIHD NMR spectrometer (Bruker) operating at a ^1H Larmor frequency of 400 MHz. The samples were spun around the magic angle with a rate of 18 kHz at room temperature using N_2(g) for the drive, bearing and VT flow. A double resonance 3.2 mm probe (with the rotor containing ca. 15 mg sample) was tuned to 100.64 or 105.22 MHz for the ^{13}C and ^{51}V experiments, respectively. The ppm scale of the spectra was calibrated using the ^{13}C signal of adamantane as an external secondary reference. All samples were packed into rotors inside a glovebox (<1 ppm of O_2 and H_2O).

Thermogravimetric analysis-differential scanning calorimetry of the calcination step was performed using a TGA-DSC Thermobalance (LINSEIS) in combination with an OmniStarTM mass spectrometer (Pfeiffer Vacuum). $V/SiO_{2(700)}$ (ca. 10 mg) was sealed in an aluminum sample pan inside a glovebox (<1 ppm of O_2 and H_2O) prior to TGA-DSC-MS analysis.

In situ Raman measurements were carried out with a Renishaw InVia Raman Spectrometer with a 785 nm excitation laser. All measurements used a 1200 l mm^{-1} grating and were taken with a range of 250−1200 cm^{-1} and a dispersion of 1.36565 cm^{-1} $pixel^{-1}$. Prior to calcinations, samples were loaded and sealed in a high-temperature Linkam CCR1000 cell inside a glovebox (<1 ppm of O_2 and H_2O) prior to measurement.

X-ray absorption near-edge structure (XANES) spectra were obtained at the V K-edge (5465.1 eV) using bending magnet station B at sector 20 of the Advanced Photon Source beamline (20-BM-B) at Argonne National Laboratory. The beam energy and detector were calibrated to the V K-edge using pure vanadium foil in transmission mode. The beam energy was controlled using a Si(111) monochromator with 1.4×10^{-4} eV resolution. Samples were pressed into a self-supporting wafer inside a helium atmosphere glovebox (<1 ppm of O_2 and H_2O), and the sample holder was sealed in a quartz tube fitted with Kapton windows on either end. All spectra were collected in transmission mode.

DOI: 10.1021/acs.chemmater.6b02118
Chem. Mater. 2016, 28, 5495−5504

Catalytic Testing. Catalytic activity measurements were performed using a Microactivity-Effi reactor. 80 mg of catalyst (particle size of 600−710 μm) was mixed with inert SiC particles of equal size in a ratio of 2:1 (SiC-to-catalyst) and packed inside a quartz reactor tube (9 mm ID). Reactions were carried out at 490 °C with inlet flow ratios of 3:6:11 O_2:C_3H_8:N_2. Exhaust streams were analyzed using a Shimadzu 2010 GC equipped with three Restek columns (Rtx-1, Rt-Q-Bond and RT-Msieve 5A) and a Thermal Conductivity Detector (TCD) and Flame Ionization Detector (FID). The catalysts were investigated under different contact times to monitor product selectivity at varying propane conversions (inverse weight-hour-space-velocity ($WHSV^{-1}$) of 40−130 [kg-cat s m^{-3}]). The carbon balance closes within 2%.

RESULTS AND DISCUSSION

Grafting $VO(O^iPr)_3$ to Dehydrated Silica. Prior to grafting $VO(O^iPr)_3$, the silica support was dehydrated under dynamic vacuum (ca. 20 μbar) at various temperatures (i.e., 200, 500, 600, 600, 700, and 800 °C). During the grafting step, the liquid vanadium precursor $VO(O^iPr)_3$ was transferred under vacuum in the vapor phase and condensed onto $SiO_{2(X)}$ at −78 °C. The material was warmed to room temperature and then thermally post-treated at 50 °C under dynamic vacuum to remove excess precursor. The structural changes occurring during thermal dehydration of silica and during the subsequent grafting were investigated using transmission infrared (IR) spectroscopy, as summarized in Figure 1.

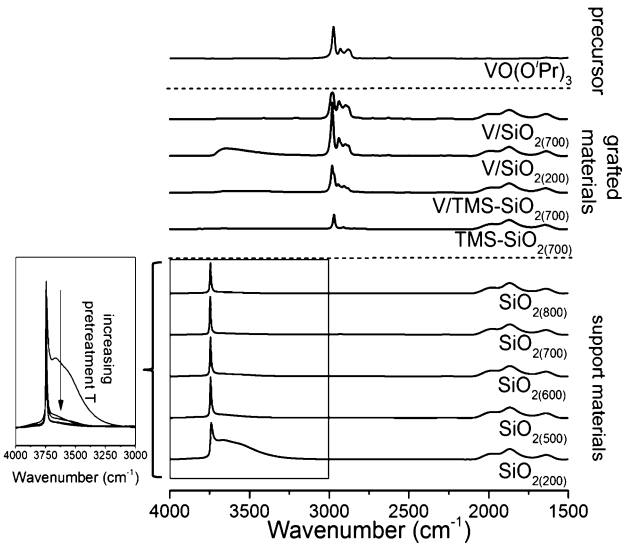

Figure 1. Transmission infrared spectra of silica dehydrated at 200, 500, 600, 700, and 800 °C ($SiO_{2(200)}$, $SiO_{2(500)}$, $SiO_{2(600)}$, $SiO_{2(700)}$, $SiO_{2(800)}$, respectively), silylated $SiO_{2(700)}$ (TMS-$SiO_{2(700)}$), $VO(O^iPr)_3$ grafted to silylated $SiO_{2(700)}$ (V/TMS-$SiO_{2(700)}$), $VO(O^iPr)_3$ grafted to $SiO_{2(200)}$ (V/$SiO_{2(200)}$) and to $SiO_{2(700)}$ (V/$SiO_{2(700)}$), and $VO(O^iPr)_3$ precursor diluted in KBr.

The IR spectrum of the silica support dehydrated at 200 °C under vacuum exhibits a sharp signal at 3740 cm^{-1} and a broad shoulder around 3666 cm^{-1} (Figure 1, $SiO_{2(200)}$). These two features are attributed to isolated and hydrogen bonded silanols, respectively.[35] The broad spectral features between 1500 and 2000 cm^{-1} in Figure 1 correspond to framework Si−O−Si overtones that were used to normalize the intensities of the different silica spectra. Upon thermal treatment under vacuum at temperatures above 600 °C, the IR spectrum of silica only shows a sharp signal at 3748 cm^{-1}, indicating that $SiO_{2(700)}$ and $SiO_{2(800)}$ feature predominantly noninteracting silanol (SiOH) groups (Figure 1, inset), in addition to a small fraction (∼5%) of geminal diols that exhibit a similar IR signature (within 2 cm^{-1}) to the isolated silanol signal.[35−37] After $VO(O^iPr)_3$ is exposed to the $SiO_{2(700)}$ support (material denoted as V/$SiO_{2(700)}$), the infrared spectrum shows several bands in the 2850 to 3000 cm^{-1} range, whereas the signal at 3748 cm^{-1} is completely consumed. From the latter, we infer that the vanadium precursor reacts quantitatively with the isolated surface silanol groups, substituting an alkoxide on the original $VO(O^iPr)_3$ vanadium precursor for a siloxide ligand according to reaction 1.

$$\equiv SiOH + VO(O^iPr)_3 \rightarrow \equiv SiO{-}VO(O^iPr)_2 + {}^iPrOH \quad (1)$$

This proposed reaction is in line with studies conducted by Guillemot and co-workers, who observe the release of isopropyl alcohol by NMR spectroscopy for the anchoring reaction of $VO(O^iPr)_3$ to a model silanol-functionalized polytungstate system.[38] Grafting to $SiO_{2(200)}$ reveals that the H-bonded SiOH groups are significantly less reactive than the isolated SiOH groups, as evidenced by the fact that the broad peak corresponding to the O−H stretch for hydrogen bonded silanols still remains in the IR spectrum for V/$SiO_{2(200)}$ (Figure 1).

In the IR spectra of $VO(O^iPr)_3$-functionalized materials in Figure 1, the bands between 2850 and 3000 cm^{-1} correspond to the C−H stretches originating from the isopropoxide ligands. Comparison of the C−H stretch fingerprint for the V/$SiO_{2(700)}$ material with the spectrum of the $VO(O^iPr)_3$ precursor reveals a difference in the relative intensities of these bands. This suggests that more complex chemistry than only that illustrated in reaction 1 might be taking place. On the basis of the isolated silanol density of $SiO_{2(700)}$ of ca. 0.9 nm^{-2}[39,40] and the determined BET surface area of ca. 186 ± 6 $m^2{\cdot}g^{-1}$, one would expect, based on a simple 1:1 stoichiometry of $VO(O^iPr)_3$ with SiOH groups, a vanadium loading of ca. 1.5 wt %. However, bulk analysis of the V/$SiO_{2(700)}$ sample indicates a vanadium loading of 2.9 ± 0.3 wt %. One plausible explanation for this anomaly is that $VO(O^iPr)_3$ reacts not only with surface silanols but also with (strained) siloxane bridges (≡Si−O−Si≡) at the silica surface, that arise as a consequence of dehydration at high temperatures under vacuum. We emphasize that the peak intensities in the C−H stretching region for the V/$SiO_{2(200)}$ material resemble the $VO(O^iPr)_3$ precursor more closely than V/$SiO_{2(700)}$, and that V/$SiO_{2(200)}$ features less strained siloxane bridges, due to the lower pretreatment temperature.[35]

To verify further the hypothesis that the $VO(O^iPr)_3$ precursor reacts with both silanol groups and siloxane bridges, we silylated $SiO_{2(700)}$, *viz*, conversion of ≡SiOH groups to $\equiv SiOSi(CH_3)_3$ (material denoted as TMS-$SiO_{2(700)}$), prior to grafting $VO(O^iPr)_3$. After $SiO_{2(700)}$ is exposed to the silylating agent *N*,*N*-bis(trimethylsilyl)methylamine ($(TMS)_2NMe$) under vacuum, the surface silanols are indeed capped with nonreactive trimethylsilyl (TMS) groups, as verified by IR spectroscopy (Figure 1, "grafted materials"). We emphasize that no nitrogen impurities could be detected with X-ray photoelectron spectroscopy (XPS), excluding a significant reaction of $(TMS)_2NMe$ with the siloxane bridges, as well as the presence of physisorbed silylating agent. We therefore conclude that when exposed to the TMS-$SiO_{2(700)}$ support, $VO(O^iPr)_3$ can only react with surface siloxane bridges, as the material has a

DOI: 10.1021/acs.chemmater.6b02118
Chem. Mater. 2016, 28, 5495−5504

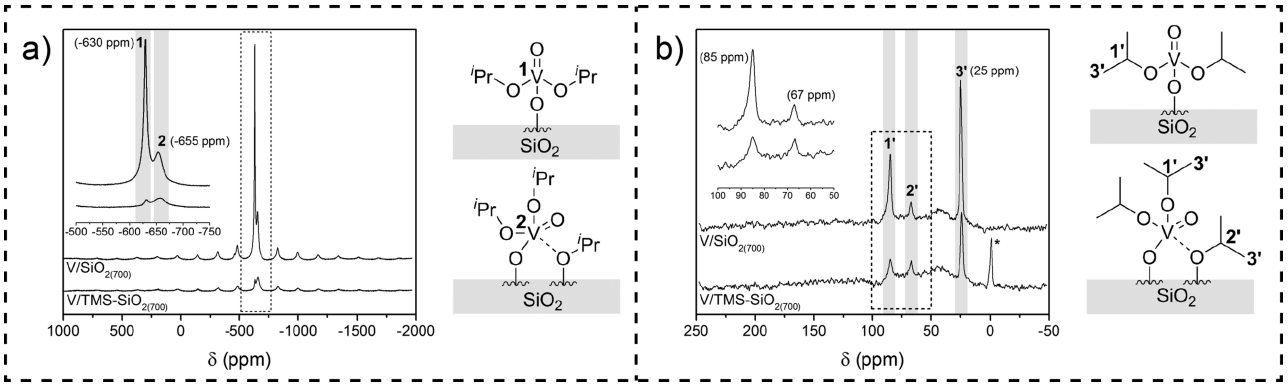

Figure 2. (a) ^{51}V MAS NMR spectra of $V/SiO_{2(700)}$ (top) and $V/TMS\text{-}SiO_{2(700)}$ (bottom), with proposed assignments for signals **1** and **2**. (b) ^{13}C MAS NMR of $V/SiO_{2(700)}$ (top) and $V/TMS\text{-}SiO_{2(700)}$ (bottom), with proposed assignments for signals **1′**, **2′**, and **3′** observed in both spectra (* Indicates the ^{13}C signal associated with TMS groups in the $V/TMS\text{-}SiO_{2(700)}$ sample introduced during the silylation).

vanadium loading ca. 0.9 ± 0.2 wt %. From this experiment, we conclude that $VO(O^iPr)_3$ can anchor to the surface of silica without the presence of silanol groups. Therefore, we interpret the anomaly in vanadium loading for $V/SiO_{2(700)}$ as evidence for the direct reaction of the $VO(O^iPr)_3$ precursor with (strained) siloxane bridges in addition to isolated silanol groups.

In contrast to the direct reaction of $VO(O^iPr)_3$ with siloxane bridges, we also consider two indirect pathways in which the anchoring of $VO(O^iPr)_3$ to siloxane bridges could occur. First, the case where the isopropyl alcohol released in reaction 1 reacts with siloxane bridges to form additional silanol grafting sites can be excluded for the case where $VO(O^iPr)_3$ is grafted to $TMS\text{-}SiO_{2(700)}$. This is due to the lack of proton source on $TMS\text{-}SiO_{2(700)}$ to protonate the isopropoxide ligands of the precursor, and therefore no proton source in which to subsequently open the siloxane bridges present on the surface. The second indirect pathway to open siloxane bridges during grafting could be the Lewis acid-catalyzed reaction of the isopropanol formed during reaction 1 with the siloxane bridges in the presence of additional $VO(O^iPr)_3$ precursor. An analogous mechanism was also previously suggested for the grafting of tin precursor $Sn(NMe_2)_4$ to $SiO_{2(700)}$.[31] The Lewis acid-catalyzed mechanism, of course, would only be plausible on $SiO_{2(700)}$ where protons are available from the surface SiOH groups. However, the vanadium-loading of $V/TMS\text{-}SiO_{2(700)}$ (where only the direct reaction of $VO(O^iPr)_3$ with siloxane bridges is likely) matches the discrepancy between the vanadium-loading of $V/SiO_{2(700)}$ and the calculated vanadium-loading that should result from quantitative reaction of $VO(O^iPr)_3$ with isolated silanols (ca. 1.5 wt % V; *vide supra*). This illustrates that grafting to siloxane bridges occurs without the presence of protons and that a Lewis acid-catalyzed pathway is thus not likely to occur for the reaction of $VO(O^iPr)_3$ with siloxane bridges.

The aforementioned experiments lead us to a first important conclusion: dispersion of vanadium oxide does not only depend on the silanol groups but also on the more hydrophobic siloxane bridges on the silica surface.

Structural Characterization of $V/SiO_{2(700)}$ and $V/TMS\text{-}SiO_{2(700)}$ with Solid-State NMR and XANES. We investigate the structure of the vanadium species on $V/SiO_{2(700)}$ and $V/TMS\text{-}SiO_{2(700)}$ using solid-state ^{51}V and ^{13}C MAS NMR (Figure 2a,b, respectively). The ^{51}V MAS NMR spectra for both $V/SiO_{2(700)}$ and $V/TMS\text{-}SiO_{2(700)}$ feature two signals with shifts centered at −630 ppm (**1**) and −655 ppm (**2**). The overall lower signal intensity for the $V/TMS\text{-}SiO_{2(700)}$ sample compared to $V/SiO_{2(700)}$ is due to the difference in vanadium loading (*vide supra*). Signal **2** has significant spinning sidebands whereas signal **1** has virtually none. Fitting of the experimental spectra furthermore reveals that signal **1** has a line width of ca. 1 kHz whereas the line width of signal **2** is twice as large at ca. 2.3 kHz (see Supporting Information Figure S1 and Table S1). In addition, the fit of signal **2** reveals that it has a significantly larger Quadrupole Coupling Constant (QCC) compared to signal **1** (Table S1). It is the quadrupolar interaction that is responsible for the appearance of the spinning sidebands, as neither signal displays a significant chemical shift anisotropy. This suggests that the species associated with signal **1** are significantly more symmetric than the species that give rise to signal **2**. The lower ratio of signal **1** to signal **2** for $V/TMS\text{-}SiO_{2(700)}$ compared to $V/SiO_{2(700)}$ points toward a different site speciation that is likely due to different anchoring mechanisms that arise from the difference in available anchoring points on the $SiO_{2(700)}$ and $TMS\text{-}SiO_{2(700)}$ supports. It is important to note that the ratio of intensities between peaks **1** and **2** in these spectra give only qualitative information about the speciation differences between $V/SiO_{2(700)}$ and $V/TMS\text{-}SiO_{2(700)}$. To achieve a truly quantitative picture of the site speciation for **1** and **2** on each material, the total integrations of these spectra would have to be normalized to a known reference (such as V_2O_5) and the spectral intensities scaled to sample weight and number of acquisition scans, as has been demonstrated, for example, by Peden and co-workers on titanium nanorod-supported vanadium oxide.[19]

We assign signal **1** the to monopodal, freely rotating $\equiv SiO\text{–}VO(O^iPr)_2$ species **1** (see Figure 2a). The narrow line width of peak **1**, combined with the fact that there is minimal quadrupolar coupling, indicates that there is a negligible electric field gradient at the ^{51}V nucleus for this species. The fact that there are virtually no spinning sidebands associated with this peak means that both the quadrupole interaction and the chemical shift anisotropy are rather small, which can be explained by a dynamic environment (i.e., more rotational freedom) around the ^{51}V nucleus. We postulate that this species arises predominantly from reaction of $VO(O^iPr)_3$ with isolated SiOH groups, as the relative abundance of species **1** is significantly higher in the $V/SiO_{2(700)}$ sample.

The spinning sidebands associated with peak **2** indicate that this peak experiences an electric field gradient at the location of

DOI: 10.1021/acs.chemmater.6b02118
Chem. Mater. 2016, 28, 5495−5504

the ^{51}V nucleus and hence exhibits a significant QCC. It is a clear indication of a less symmetric environment. The chemical shift anisotropy is, however, almost absent. On the basis of this lower symmetry, as well as the minor upfield shift by 25 ppm compared to signal **1**, we attribute signal **2** to a structure where the vanadium center features a weak fifth coordination bond to an adjacent ≡Si−O^{i}Pr moiety (species **2** in Figure 2a). This perturbs the tetrahedral geometry of the vanadium site into a distorted square-pyramidal structure, whose asymmetric coordination environment is responsible for the intensity of the spinning sidebands associated with signal **2**. We postulate the magnitude of the QCC (888 kHz) in combination with negligible chemical shift anisotropy strongly supports the presence of a weak interaction for species **2**: there is sufficient rotational averaging in this species to average out contributions from chemical shift anisotropy; however, the interaction of the ^{51}V nucleus with the adjacent ≡Si−O^{i}Pr site reduces the symmetry about the ^{51}V nucleus to the point where strong quadrupolar interactions (responsible for the spinning sidebands) are still prevalent. In addition, we emphasize that the additional weak coordination bond slightly increases the electron density at the vanadium nucleus, causing the subtle shielding effect compared to signal **1**. As the relative abundance of peak **2** is much higher in the silylated material V/TMS-$SiO_{2(700)}$, we assume that species **2** is mainly formed in the reaction of $VO(O^iPr)_3$ with strained siloxane bridges.

Alternative structures that would feature a high degree of anisotropy (either quadrupolar or chemical shift), and could hence potentially explain signal **2** in the ^{51}V NMR spectra, are the two bipodal species in Scheme 1 (labeled **2bis** and **2tris**).

Scheme 1. Possible Structures for the Species Experimentally Observed in ^{51}V MAS NMR[a]

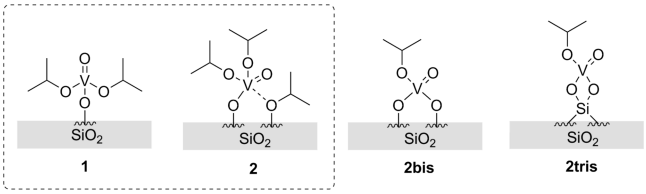

[a]From left to right: monopodal species **1**, distorted monopodal vanadium species with a weak fifth coordination to an adjacent Si−O^{i}Pr moiety (species **2**), bipodal vanadium with two surface Si−O−V bonds (=Si$(OH)_2$; species **2bis**), and geminal bipodal vanadium species that could arise from subsequent grafting to geminal (>Si$(OH)_2$) silanol groups (species **2tris**).

Indeed, the anchoring of one $VO(O^iPr)_3$ molecule to two isolated silanols at sufficiently close proximity to one another would yield the $(\equiv SiO)_2VO(O^iPr)$ species **2bis**. In addition, approximately 5% of the silanols on $SiO_{2(700)}$ are present as geminal diols,[35] and grafting to those >Si$(OH)_2$ groups could yield the >$SiO_2VO(O^iPr)$ species **2tris**. Although the former seems unlikely at a silanol surface coverage of only 0.9 nm^{-2} for $SiO_{2(700)}$, local deviations from a pure statistical distribution could indeed cause the formation of such bipodal species. However, we emphasize that such mechanisms are not possible in the absence of silanols, and that signal **2** is also observed, and even in a higher relative abundance to signal **1**, on V/TMS-$SiO_{2(700)}$, where all silanols on the support are capped on the TMS-$SiO_{2(700)}$ support prior to grafting. In addition, the fact that only quadrupolar interaction (and no chemical shift anisotropy) is observed for signal **2** in ^{51}V NMR does not support the presence of species **2bis** or **2tris**. Both species **2bis** and **2tris** have two surface bonds to silica, meaning that elimination of contributions from chemical shift anisotropy via rotational averaging is virtually impossible. **2bis** and **2tris** would likely have significant contributions from both chemical shift anisotropy and quadrupolar coupling, which would manifest itself in much more pronounced spinning sidebands, such as those observed for dispersed vanadium oxide species on silica after calcination.[18]

The ^{13}C MAS NMR spectra for V/$SiO_{2(700)}$ and V/TMS-$SiO_{2(700)}$ in Figure 2b share three chemical shifts at 85 ppm (**1′**), 67 ppm (**2′**), and 25 ppm (**3′**). V/TMS-$SiO_{2(700)}$ also has a peak at −0.86 ppm arising from surface TMS groups. The signal at 25 ppm corresponds to primary methyl groups in the isopropoxide ligands. Signals **1′** and **2′** are in the chemical shift range of the tertiary carbon directly bound to the oxygen in the isopropoxide ligand and are assigned to V−O^{i}Pr and Si−O^{i}Pr, respectively, based on the deshielding expected for the V−O^{i}Pr tertiary carbon relative to the Si−O^{i}Pr tertiary carbon. The Si−O^{i}Pr species most likely arise from transfer of one of the $VO(O^iPr)_3$ isopropoxide ligands to the silica surface during grafting to siloxane bridges (see Scheme 2). These ^{13}C NMR

Scheme 2. Possible Reactions of the $VO(O^iPr)_3$ Precursor with Isolated Silanol and Siloxane Bridge Sites, Respectively

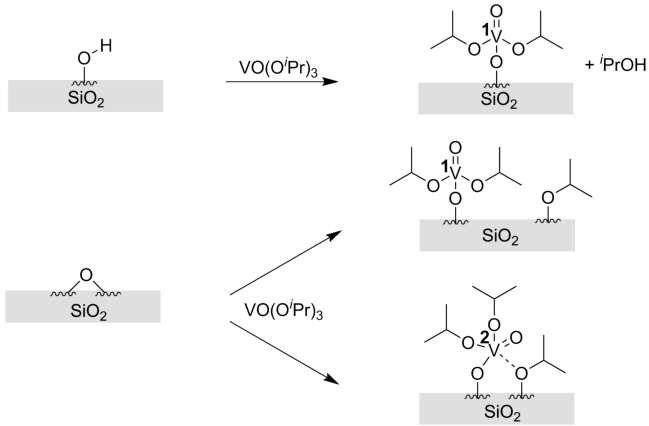

spectra also allow us to further reject the bipodal structures hypothesized in Scheme 1. Indeed, if we assume that the two tertiary carbon signals from the Si−O^{i}Pr and V−O^{i}Pr moieties (signals **1′** and **2′**, Figure 2b) have a similar extinction coefficient due to their similar chemical environment, integration of these two peaks allows us to estimate their relative abundance at ca. 2:1 for the V/TMS-$SiO_{2(700)}$ material. This observation is only consistent with the formation of the distorted square-pyramidal structure **2** in Scheme 1. Indeed, in both bipodal cases drawn in Scheme 1, the vanadium site only contains one isopropoxide ligand; whereas in case of the distorted square-pyramidal species, the vanadium site maintains two native isopropoxide ligands in addition to one ≡Si−O^{i}Pr species.

The assignment of signals **1** and **2** in ^{51}V MAS NMR also agrees with analysis of the XANES region of the XAS spectra reported in the Supporting Information (Figure S2, panel a). Indeed, the normalized pre-edge in the XANES spectra of the vanadium K-edge can be correlated with the local environment of vanadium. The normalized XANES region for V/$SiO_{2(700)}$, V/TMS-$SiO_{2(700)}$, and reference material $VO(OSiPh_3)_3$ all have

DOI: 10.1021/acs.chemmater.6b02118
Chem. Mater. 2016, 28, 5495−5504

pre-edge transitions at approximately 5469 eV. On the basis of the combination of XANES and ^{51}V MAS NMR analyses, we postulate the vanadium sites on V/$SiO_{2(700)}$ and V/TMS-$SiO_{2(700)}$ have predominantly tetrahedral geometry. However, although the energy of the pre-edge peak is effectively the same for V/$SiO_{2(700)}$ and $VO(OSiPh_3)_3$, the normalized absorption intensity of the pre-edge peak is higher for V/TMS-$SiO_{2(700)}$. We attribute this increase in intensity to an increase in the quadrupolar coupling of the vanadium nuclei, which in turn reflects the more asymmetric environment of vanadium in the silylated sample. This supports the conclusions drawn from the ^{51}V MAS NMR studies, which show a much higher relative abundance of the asymmetric species **2** (with a higher quadrupolar coupling constant) for the V/TMS-$SiO_{2(700)}$ material. Although the intensity of the normalized pre-edge peak for V/TMS-$SiO_{2(700)}$ is higher, the peak position does not shift. This observation appears to indicate that although the vanadium sites, on average, are in a more distorted configuration, they remain predominantly tetrahedrally coordinated. On the other hand, if the local environment of vanadium restructured into a truly pentacoordinated configuration, the intensity of the pre-edge peak would decrease, rather than increase.[41] All of these observations are in line with the proposed vanadium structure **2** in Scheme 1.

We now return to the observation that both the symmetric (signal **1**) and asymmetric (signal **2**) species are observed with ^{51}V NMR on V/TMS-$SiO_{2(700)}$ (see Figure 2a). To investigate this in more detail, we grafted vanadium to silylated silica that was pretreated at different temperatures (500−800 °C). From the ^{51}V NMR spectra displayed in Figure 3, one can conclude

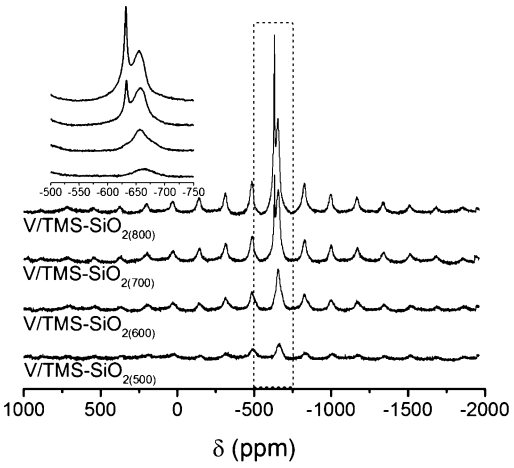

Figure 3. ^{51}V MAS NMR spectra of V/TMS-$SiO_{2(500)}$, V/TMS-$SiO_{2(600)}$, V/TMS-$SiO_{2(700)}$, and V/TMS-$SiO_{2(800)}$.

that the relative abundance of previously assigned species **1** and **2** changes drastically with dehydration temperature. These observations point toward the almost exclusive formation of asymmetric vanadium species of type **2** on the silylated silica pretreated at temperatures up to 600 °C. At higher pretreatment temperatures, more symmetric (tetrahedral) vanadium species of type **1** are generated, in addition to the type **2** species. Clearly, the coordination environment of the grafted vanadium species is very sensitive to the changes in the silica surface that occur during thermal treatment. This effect correlates with the formation of more strained siloxane bridges at higher pretreatment temperatures (>600 °C), due to more extensive dehydroxylation of the surface hydroxyl species.[35] The more strained siloxane bridges seem to react with the $VO(O^iPr)_3$ precursor to form the isolated tetrahedral sites, and react in such a way as to minimize ring strain on the silica surface.

From this series of solid-state NMR and XANES studies, we conclude that the grafting of $VO(O^iPr)_3$ to silica leads to the formation of two types of surface species, one monopodal species (**1**, Figure 1a) that is tetrahedral and one distorted tetrahedral species with a fifth additional weak interaction with a neighboring ≡Si—O—^{i}Pr group (**2**, Figure 2a). When grafting to siloxane bridges only, the relative abundance of species **1** and **2** depends on the pretreatment temperature of the silica.

Thermal Restructuring of Vanadium Sites During Calcination of V/$SiO_{2(700)}$. After the grafting step, V/$SiO_{2(700)}$ was calcined under air flow (20 mL·min^{-1}) at 600 °C to yield the material V/$SiO_{2(700)}$-O_2. This step was monitored using *in situ* DRIFTS. The temperature-dependent IR spectra are displayed in Figure 4. Upon heating, the intensity

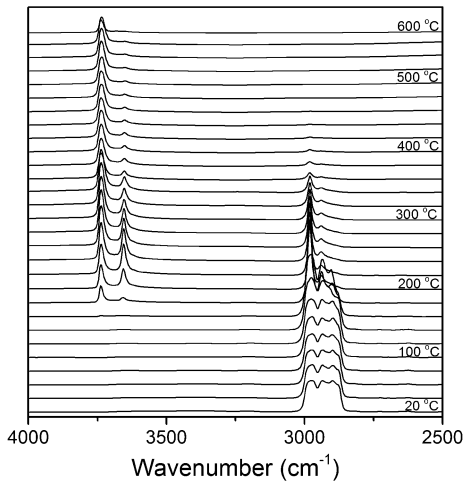

Figure 4. *In situ* DRIFTS study of the calcination of V/$SiO_{2(700)}$ (ramp rate of 20 °C min^{-1} under air).

of the IR signals from the organic ligands (2850−3000 cm^{-1}) gradually decreases and eventually vanishes above 400 °C. At approximately 200 °C, signals at 3738 and 3656 cm^{-1} start to appear which we attribute to SiO−H and VO−H stretches, respectively.[7] The transient behavior of the VO−H species identifies them as an intermediate in the restructuring process. After completion of the calcination, only trace amounts of the SiO−H signal remain in the IR spectrum.

The calcination of V/$SiO_{2(700)}$ was also monitored using coupled thermogravimetric analysis-differential scanning calorimetry-mass spectrometry (TGA-DSC-MS). Figure 5a overlays the measured mass loss and change in heat flow with respect to temperature during the calcination as measured by TGA and DSC, respectively. At 225−230 °C, a sharp endothermic transition is observed in the DSC trace, and a sharp decrease in mass is observed in the TGA trace. When coupled with the MS data (Figure 5b), it appears that mass fragments corresponding to propene (m/z = 42) and water (m/z = 18) both appear in the temperature range of 225−250 °C.

Complementary information on the calcination process of V/$SiO_{2(700)}$ was obtained by *in situ* Raman spectroscopy (Figure 6). The results indicate that the V═O (vanadyl) stretch

DOI: 10.1021/acs.chemmater.6b02118
Chem. Mater. 2016, 28, 5495−5504

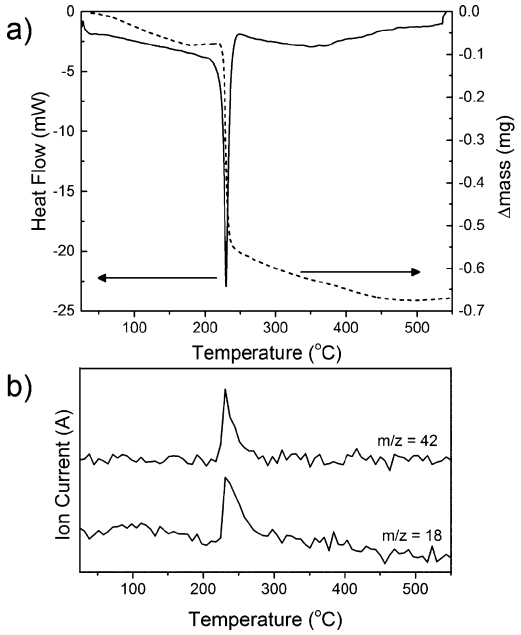

Figure 5. (a) TGA (right axis) and DSC (left axis) traces as a function of temperature for the calcination of 10 ± 0.1 mg $V/SiO_{2(700)}$ under air. (b) Evolution of the propylene and water signals observed with MS as a function of the calcination temperature.

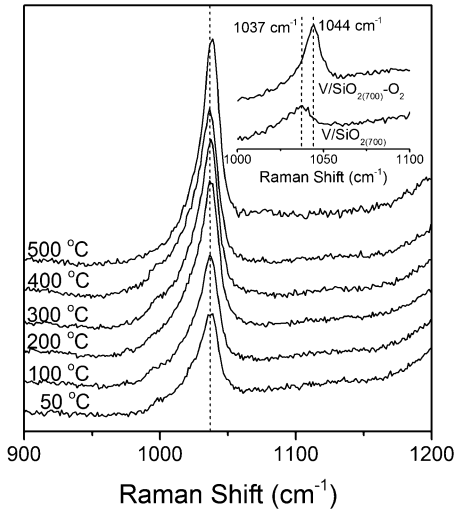

Figure 6. *In situ* Raman spectra of $V/SiO_{2(700)}$ during calcination in air, as well as Raman spectra of $V/SiO_{2(700)}$ before and after calcinations, both taken at 25 °C (inset).

characteristic for dispersed vanadium at ca. 1037 cm^{-1} is preserved throughout the entire calcination.[10,11] Comparison of the uncalcined $V/SiO_{2(700)}$ and calcined $V/SiO_{2(700)}$-O_2 at room temperature shows a shift in the vanadyl stretch from 1037 to 1044 cm^{-1}, respectively (Figure 6, inset), which is likely due to the slight change in vanadyl stretch environment upon formation of multiple Si−O−V surface bonds during calcination. A Raman shift between 983 and 998 cm^{-1} was never observed, indicating that no vanadium oxide nanoparticles are generated.[10,11]

Scheme 3 summarizes our hypothesized pathways by which vanadium sites on $V/SiO_{2(700)}$ restructure upon calcination, based on observations from our DRIFTS, TGA-DSC-MS, and Raman experiments. In the first step, the isopropoxide ligands from both V−O−^{i}Pr and Si−O−^{i}Pr moieties decompose to propene (observed by mass spectrometry), which also in turn corresponds to the decrease in organic signal in the DRIFTS spectra. Upon the elimination of propene, Si—OH and V−OH species are formed. A proposed mechanism is given for the formation of V−OH species in which the vanadyl moiety abstracts a proton from an adjacent methyl group. Through a cyclic six-membered transition state, the three carbons from the isopropoxide ligand leave as propene and a V−OH group remains. We emphasize that this mechanism is in line with the observation that the V═O stretch is conserved throughout the calcination process as demonstrated by *in situ* Raman spectroscopy.

In the second step of Scheme 3, the initial surface Si−O−V linkages are formed by via a condensation reaction between nearby V−OH and Si−OH groups formed in the first step outlined in Scheme 3. This is evidenced by the transient behavior of the Si−OH and V−OH species in DRIFTS (Figure S3), as well as by the fact that the release of water is observed in concert with a significant endothermic reaction in the TGA-DSC-MS data (Figure 5). Given the low density of Si−OH groups on the surface during calcination, further Si−O−V linkages are likely formed from the reaction of V−OH groups with adjacent Si−O−Si bridges, which is supported by the fact that Si−OH groups (formed from the transfer of the V−OH group proton to open the Si−O−Si linkage) are still observed in DRIFTS at the end of the calcination.

Characterization of Calcined $V/SiO_{2(700)}$-O_2. Both $V/SiO_{2(700)}$ and $V/TMS\text{-}SiO_{2(700)}$ were calcined in air at 600 °C to yield materials denoted $V/SiO_{2(700)}$-O_2 and $V/TMS\text{-}SiO_{2(700)}$-$O_2$, respectively. The ^{51}V MAS NMR spectra of dehydrated $V/SiO_{2(700)}$-O_2 and $V/TMS\text{-}SiO_{2(700)}$-$O_2$ are shown in Figure 7. A single isotropic shift is observed at −694 ppm for both samples. This indicates the formation of similar vanadium species in both materials, albeit at a different surface densities. The very intense spinning sidebands point toward a nondynamic chemical environment for these sites, which precludes a dynamic averaging of the local environment of the ^{51}V nucleus and leads to the inhomogeneously broadened peaks observed in the spectrum. We therefore attribute this signal to a tetrahedral VO_4 species with three Si−O−V linkages to the silica surface and one single V═O group (proposed structure inset in Figure 7). Previous work by Baiker and co-workers on vanadium oxide/silica materials assigns ^{51}V NMR shifts for monomeric tetrahedral VO_4 species to an isotropic shift at ca. −715 ppm, and distorted tetrahedral VO_4 sites at ca. −691 ppm.[18] We would expect the observed shift at −694 ppm for $V/SiO_{2(700)}$-O_2 and $V/TMS\text{-}SiO_{2(700)}$-$O_2$ to have a distorted tetrahedral geometry as well, due to the amorphous nature of the silica support. As a comparison, we also measured the ^{51}V MAS NMR isotropic shift of tris(triphenylsiloxy) vanadium oxide ($VO(OSiPh_3)_3$), to be −720 ppm (Figure 7 inset, spectrum in Figure S4), in order to replicate a previous study on model compounds for silica-supported vanadium oxide.[9] The chemical shift observed for $V/SiO_{2(700)}$-O_2 and reference compound $VO(OSiPh_3)_3$, in combination with previous literature[9,15,18] appears to indicate clearly the presence of solely isolated VO_4 species with bonds only to the silica surface, and no oligomeric species with V−O−V linkages. These structural assignments were also verified by analysis of the pre-edge peak in the vanadium K-edge XANES spectra (Figure S2, panel b) for $V/SiO_{2(700)}$-O_2 and $V/TMS\text{-}SiO_{2(700)}$-$O_2$. The normalized pre-edge peak intensity for the tetrahedral, four-fold oxygen

DOI: 10.1021/acs.chemmater.6b02118
Chem. Mater. 2016, 28, 5495−5504

Scheme 3. Proposed Reconstruction Pathway for Vanadium Sites on $V/SiO_{2(700)}$ upon Calcination[a]

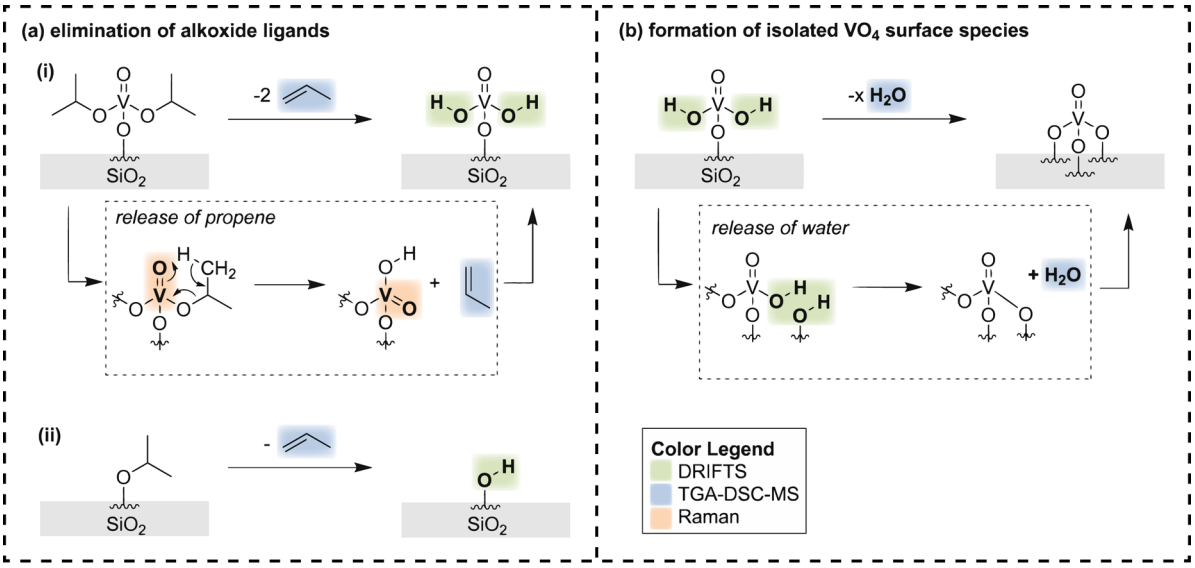

[a]Various bonds and molecules are highlighted to indicate the experiment from which they were initially observed (see legend in figure). Based on *in situ* DRIFTS, TGA-DSC-MS, and Raman studies the restructuring process involves (a) the elimination of alkoxide ligands in the form of propene from both (i) V−O−^{i}Pr and (ii) Si−O−^{i}Pr moieties, and (b) the formation of multipodal species on the silica surface by reaction of V− OH groups with silanol groups generated during calcination. It is important to note that processes (a) and (b) do not occur consecutively, but rather in concert with one another as suggested by TGA-DSC-MS and DRIFTS.

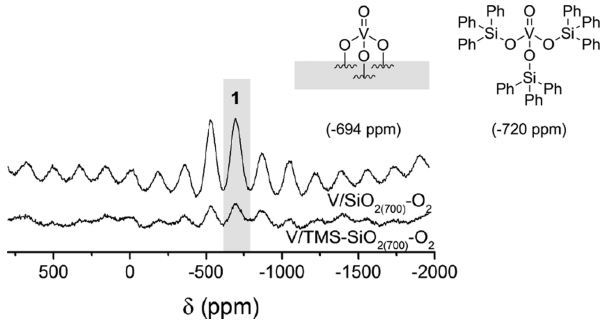

Figure 7. ^{51}V MAS NMR spectra of calcined materials $V/SiO_{2(700)}$-O_2 (top) and $V/TMS\text{-}SiO_{2(700)}$-$O_2$ (bottom) All calcinations were done at 600 °C in air. Prior to NMR analysis, samples were dehydrated at 300 °C under vacuum to remove any physisorbed water. Inset structures correspond to the assignment of the single isotropic shift observed in both spectra (left) and the reference material for tetrahedrally coordinated vanadium species and its associated chemical shift (right).

coordinated $VO(OSiPh_3)_3$ reference, $V/SiO_{2(700)}$-O_2 and $V/TMS\text{-}SiO_{2(700)}$-$O_2$ materials are all nearly identical, which is indicative of similar local coordination environments for each material. On the basis of these NMR and XANES data for $V/SiO_{2(700)}$-O_2 and $V/TMS\text{-}SiO_{2(700)}$-$O_2$, we also conclude that the calcined surface species that arise from the initial reaction of $VO(O^iPr)_3$ with both silanols and strained siloxane bridges result in structurally similar surface species.

Oxidative Dehydrogenation of Propane as Catalytic Test Reaction. The oxidative dehydrogenaton of propane (ODHP) is a structure-sensitive reaction. Indeed, it is well established in the literature that consecutive overoxidation of the desired propylene is enhanced by the presence of three-dimensional V_2O_5 particles.[1,4] When comparing the performance of our $V/SiO_{2(700)}$-O_2 material with an analogous material obtained via incipient wetness impregnation featuring the same vanadium loading (as well as the same vanadium coverage nm^{-2}), very similar turnover frequencies were obtained: 0.0145 and 0.0163 s^{-1}, respectively, at 490 °C. Also, propene selectivity at a given propane conversion for dispersed vanadium oxide prepared by grafting and incipient wetness impregnation is in perfect agreement (Figure S5).[42] We interpret these observations as complementary catalytic evidence for the fact that we obtained solely two-dimensional VO_X surface species, and that analogous sites are formed irrespective of the synthesis procedure.

CONCLUSIONS

In this contribution, we use grafting as a tool to understand the key chemical reactions that occur during (i) the anchoring of $VO(O^iPr)_3$ to dehydrated silica, as well as (ii) the calcination of the material to form supported metal oxide sites. When $VO(O^iPr)_3$ is grafted to $SiO_{2(700)}$, it reacts with both isolated silanols and strained siloxane bridges, as determined through a combination of ICP and transmission FT-IR analyses. The uncalcined material has two distinct surface sites as determined by ^{13}C and ^{51}V MAS NMR and verified by XANES. *In situ* DRIFTS, TGA-DSC-MS, and Raman studies on the calcination of $V/SiO_{2(700)}$ reveal the elimination of isopropoxide ligands as propene to form transient V−OH species, which then react with the silica surface to form isolated, tetrahedral VO_4 sites. ^{51}V MAS NMR of the calcined silylated and nonsilylated materials shows that both original vanadium species observed in the ^{51}V MAS NMR spectra result in the formation of similar surface sites after calcination.

The methodology used for the $V/SiO_{2(700)}$ system can be extended toward a more generalized understanding of surface species that arise from grafting with molecular precursors. An increased understanding of the surface reactions that occur at the molecular level of these supported materials can open avenues for new strategies for enhanced dispersion of desired two-dimensional metal or metal oxide sites on a support material.

DOI: 10.1021/acs.chemmater.6b02118
Chem. Mater. 2016, 28, 5495−5504

■ ASSOCIATED CONTENT

Supporting Information

The Supporting Information is available free of charge on the ACS Publications website at DOI: 10.1021/acs.chemmater.6b02118.

Simulated ^{51}V MAS NMR spectrum, XANES data, deconvolution of DRIFTS data, ^{51}V NMR spectrum for $VO(SiOPh_3)_3$, ODHP activity data, table of fitting parameters from simulated ^{51}V NMR spectra, table of BET surface area and vanadium ICP data (PDF).

■ AUTHOR INFORMATION

Corresponding Author

*Ive Hermans. Email: hermans@chem.wisc.edu.

Notes

The authors declare no competing financial interest.

■ ACKNOWLEDGMENTS

The authors acknowledge financial support from the University of Wisconsin-Madison. This research used resources of the Advanced Photon Source, a U.S. Department of Energy (DOE) Office of Science User Facility operated for the DOE Office of Science by Argonne National Laboratory under Contract No. DE-AC02-06CH11357. We specifically acknowledge support from Sam Burt and beamline engineer Dale Brewe, who assisted in the collection of XANES data reported in this publication.

■ REFERENCES

(1) Carrero, C. A.; Schloegl, R.; Wachs, I. E.; Schoemaecker, R. Critical Literature Review of the Kinetics for the Oxidative Dehydrogenation of Propane over Well-Defined Supported Vanadium Oxide Catalysts. *ACS Catal.* **2014**, *4*, 3357−3380.

(2) Wachs, I. E.; Deo, G.; Weckhuysen, B. M.; Andreini, A.; Vuurman, M. A.; de Boer, M.; Amiridis, M. D. Selective Catalytic Reduction of NO with NH_3 over Supported Vanadia Catalysts. *J. Catal.* **1996**, *161*, 211−221.

(3) Busca, G.; Lietti, L.; Ramis, G.; Berti, F. Chemical and mechanistic aspects of the selective catalytic reduction of NO_x by ammonia over oxide catalysts: A review. *Appl. Catal., B* **1998**, *18*, 1−36.

(4) Carrero, C. A.; Keturakis, C. J.; Orrego, A.; Schomacker, R.; Wachs, I. E. Anomalous reactivity of supported V_2O_5 nanoparticles for propane oxidative dehydrogenation: influence of the vanadium oxide precursor. *Dalton Trans.* **2013**, *42*, 12644−12653.

(5) Bulánek, R.; Čapek, L.; Setnička, M.; Čičmanec, P. DR UV-vis Study of the Supported Vanadium Oxide Catalysts. *J. Phys. Chem. C* **2011**, *115*, 12430−12438.

(6) Nitsche, D.; Hess, C. Structure of Isolated Vanadia and Titania: A Deep UV Raman, UV-Vis, and IR Spectroscopic Study. *J. Phys. Chem. C* **2016**, *120*, 1025−1037.

(7) Keller, D. E.; Visser, T.; Soulimani, F.; Koningsberger, D. C.; Weckhuysen, B. M. Hydration effects on the molecular structure of silica-supported vanadium oxide catalysts: A combined IR, Raman, UV-vis and EXAFS study. *Vib. Spectrosc.* **2007**, *43*, 140−151.

(8) Xie, S.; Iglesia, E.; Bell, A. T. Effects of Temperature on the Raman Spectra and Dispersed Oxides. *J. Phys. Chem. B* **2001**, *105*, 5144−5152.

(9) Das, N.; Eckert, H.; Hu, H.; Wachs, I. E.; Walzer, J. F.; Feher, F. J. Bonding states of surface vanadium(V) oxide phases on silica: structural characterization by vanadium-51 NMR and Raman spectroscopy. *J. Phys. Chem.* **1993**, *97*, 8240−8243.

(10) Lee, E. L.; Wachs, I. E. In Situ Spectroscopic Investigation of the Molecular and Electronic Structures of SiO_2 Supported Surface Metal Oxides. *J. Phys. Chem. C* **2007**, *111*, 14410−14425.

(11) Lee, E. L.; Wachs, I. E. In Situ Raman Spectroscopy of SiO_2-Supported Transition Metal Oxide Catalysts: An Isotopic ^{18}O-^{16}O Exchange Study. *J. Phys. Chem. C* **2008**, *112*, 6487−6498.

(12) Silversmit, G.; van Bokhoven, J. A.; Poelman, H.; van der Eerden, A. M. J.; Marin, G. B.; Reyniers, M.-F.; De Gryse, R. The structure of supported and unsupported vanadium oxide under calcination, reduction and oxidation determined with XAS. *Appl. Catal., A* **2005**, *285*, 151−162.

(13) Szeto, K. C.; Loges, B.; Merle, N.; Popoff, N.; Quadrelli, A.; Hongpeng, J.; Berrier, E.; De MallMann, A.; Delevoye, L.; Gauvin, R. M.; Taoufik, M. Vanadium Oxo Organometallic Species Supported on Silica for the Selective Non-oxidative Dehydrogenation of Propane. *Organometallics* **2013**, *32*, 6452−6460.

(14) Thornburg, N. E.; Thompson, A. B.; Notestein, J. M. Periodic Trends in Highly Dispersed Groups IV and V Supported Metal Oxide Catalysts for Alkene Epoxidation with H_2O_2. *ACS Catal.* **2015**, *5*, 5077−5088.

(15) Centi, G.; Perathoner, S.; Trifiro, F.; Aboukais, A.; Aissi, C. F.; Guelton, M. Physicochemical characterization of V-silicalite. *J. Phys. Chem.* **1992**, *96*, 2617−2629.

(16) Eckert, H.; Wachs, I. E. Solid-State ^{51}V NMR Structural Studies on Supported Vanadium(V) Oxide Catalysts: Vanadium Oxide Surface Layers on Alumina and Titania Supports. *J. Phys. Chem.* **1989**, *93*, 6796−6805.

(17) Klug, C. A.; Kroeker, S.; Aguiar, P. M.; Zhou, M.; Stec, D. F.; Wachs, I. E. Insights into Oxygen Exchange Between Gaseous O_2 and Supported Vanadium Oxide Catalysts via ^{17}O NMR. *Chem. Mater.* **2009**, *21*, 4127−4134.

(18) Schimmoeller, B.; Jiang, Y.; Pratsinis, S. E.; Baiker, A. Structure of flame-made vanadia/silica and catalytic behavior in the oxidative dehydrogenation of propane. *J. Catal.* **2010**, *274*, 64−75.

(19) Hu, J. Z.; Xu, S.; Li, W.-Z.; Hu, M. Y.; Deng, X.; Dixon, D. A.; Vasiliu, M.; Craciun, R.; Wang, Y.; Bao, X.; Peden, C. H. F. Investigation of the Structure and Active Sites of TiO_2 Nanorod Supported VO_x Catalysts by High-Field and Fast-Spinning ^{51}V MAS NMR. *ACS Catal.* **2015**, *5*, 3945−3952.

(20) Pinna, F. Supported metal catalysts preparation. *Catal. Today* **1998**, *41*, 129−137.

(21) Marceau, E.; Carrier, X.; Che, M.; Clause, O.; Marcilly, C. Ion Exchange and Impregnation. In *Handbook of Heterogeneous Catalysis*; Wiley-VCH: Weinheim, Germany, 2008; 2:2.4:2.4.2, pp 467−484.

(22) Ajjou, J. A. N.; Rice, G. L.; Scott, S. L. Kinetics and Mechanisms of Thermally Induced Alkane Eliminations from Silica-Supported Bis(alkyl)chromium(IV) and -vanadium(IV) Complexes. *J. Am. Chem. Soc.* **1998**, *120*, 13436−13443.

(23) Mania, P.; Conrad, S.; Verel, R.; Hammond, C.; Hermans, I. Thermal restructuring of silica-grafted -CrO_2Cl and -$VOCl_2$ species. *Dalton Trans.* **2013**, *42*, 12725−12732.

(24) Mania, P.; Verel, R.; Jenny, F.; Hammond, C.; Hermans, I. Thermal Restructuring of Silica-Grafted $TiCl_x$ Species and Consequences for Epoxidation Catalysis. *Chem. - Eur. J.* **2013**, *19*, 9849−9858.

(25) Wegener, S. L.; Kim, H.; Marks, T. J.; Stair, P. C. Precursor Nuclearity Effects in Supported Vanadium Oxides Prepared by Organometallic Grafting. *J. Phys. Chem. Lett.* **2011**, *2*, 170−175.

(26) Zhu, H.; Ould-Chikh, S.; Dong, H.; Llorens, I.; Saih, Y.; Anjum, D. H.; Hazemann, J.-L.; Basset, J.-M. VO_x/SiO_2 Catalyst Prepared by Grafting $VOCl_3$ on Silica for Oxidative Dehydrogenation of Propane. *ChemCatChem* **2015**, *7* (20), 3332−3339.

(27) Keranen, J.; Auroux, A.; Ek, S.; Niinisto, L. Preparation, characterization and activity testing of vanadia catalysts deposited onto silica and alumina supports by atomic layer deposition. *Appl. Catal., A* **2002**, *228*, 213−225.

(28) Keranen, J.; Guimon, C.; Iiskola, E.; Auroux, A.; Niinisto, L. Surface-Controlled Gas-Phase Deposition and Characterization of Highly Dispersed Vanadia on Silica. *J. Phys. Chem. B* **2003**, *107*, 10773−10784.

(29) Gervasini, A.; Carniti, P.; Keränen, J.; Niinisto, L.; Auroux, A. Surface Characteristics and activity in selective oxidation of *o*-xylene of

DOI: 10.1021/acs.chemmater.6b02118
Chem. Mater. 2016, 28, 5495−5504

supported V_2O_5 catalysts prepared by standard impregnation and atomic layer deposition. *Catal. Today* **2004**, *96*, 187−194.
(30) Keranen, J.; Carniti, P.; Gervasini, A.; Iiskola, E.; Auroux, A.; Niinisto, L. Preparation by atomic layer deposition and characterization of active sites in nanodispersed vanadia/titania/silica catalysts. *Catal. Today* **2004**, *91*−*92*, 67−71.
(31) Conrad, S.; Verel, R.; Hammond, C.; Wolf, P.; Göltl, F.; Hermans, I. Silica-Grafted Sn^{IV} Catalysts in Hydrogen-Transfer Reactions. *ChemCatChem* **2015**, *7*, 3270−3278.
(32) Conley, M. P.; Rossini, A. J.; Comas-Vives, A.; Valla, M.; Casano, G.; Ouari, O.; Tordo, P.; Lesage, A.; Emsley, L.; Copéret, C. Silica-surface reorganization during organotin grafting evidenced by ^{119}Sn DNP SENS: a tandem reaction of *gem*-silanols and strained siloxane bridges. *Phys. Chem. Chem. Phys.* **2014**, *16*, 17822−17827.
(33) Wegener, S. L.; Marks, T. J.; Stair, P. C. Design Strategies for the Molecular Level Synthesis of Supported Catalysts. *Acc. Chem. Res.* **2012**, *45*, 206−214.
(34) Adachi, M.; Lefebvre, F.; Basset, J.-M. Surface Organometallic Chemistry of Tin: Grafting Reactions on Highly Dehydroxylated Silica. *Chem. Lett.* **1996**, 221−222.
(35) Zhuravlev, L. T. The surface chemistry of amorphous silica. Zhuravlev model. *Colloids Surf., A* **2000**, *173*, 1−38.
(36) Hoffmann, P.; Knozinger, E. Novel aspects of mid and far IR Fourier spectroscopy applied to surface and adsorption studies on SiO_2. *Surf. Sci.* **1987**, *188*, 181−198.
(37) Rimola, A.; Costa, D.; Sodupe, M.; Lambert, J.-F.; Ugliengo, P. Silica Surface Features and Their Role in the Adsorption of Biomolecules: Computational Modeling and Experiments. *Chem. Rev.* **2013**, *113*, 4216−4313.
(38) Guillemot, G.; Matricardi, E.; Chamoreau, L. M.; Thouvenot, R.; Proust, A. Oxidovanadium(V) Anchored to Silanol-Functionalized Polyoxotungstates: Molecular Models for Single-Site Silica-Supported Vanadium Catalysts. *ACS Catal.* **2015**, *5*, 7415−7423.
(39) Gajan, D.; Copéret, C. Silica-supported single-site catalysts: to be or not to be? A conjecture on silica surfaces. *New J. Chem.* **2011**, *35*, 2403−2408.
(40) Rascon, F.; Wischert, R.; Copéret, C. Molecular nature of support effects in single-site heterogeneous catalysts: silica *vs.* alumina. *Chem. Sci.* **2011**, *2*, 1449−1456.
(41) Yamamoto, T. Assignment of pre-edge peaks in K-edge x-ray absorption spectra of 3d transition metal compounds: electric dipole or quadrupole? *X-Ray Spectrom.* **2008**, *37*, 572−584.
(42) Grant, J. T.; Carrero, C. A.; Love, A. M.; Verel, R.; Hermans, I. Enhanced Two-Dimensional Dispersion of Group V Metal Oxides on Silica. *ACS Catal.* **2015**, *5*, 5787−5793.

DOI: 10.1021/acs.chemmater.6b02118
Chem. Mater. 2016, 28, 5495−5504